RESISTIVITY MODELLING FOR ARBITRARILY SHAPED TWO-DIMENSIONAL STRUCTURES *

BY

A. DEY and H. F. MORRISON **

ABSTRACT

DEY, A., and MORRISON, H. F., 1979, Resistivity Modelling for Arbitrarily Shaped Two-Dimensional Structures, Geophysical Prospecting 27, 106-136.

A numerical technique is developed to solve the three-dimensional potential distribution about a point source of current located in or on the surface of a half-space containing arbitrary two-dimensional conductivity distribution. Finite difference equations are obtained for Poisson's equations by using point- as well as area-discretization of the subsurface. Potential distributions at all points in the set defining the half-space are simultaneously obtained for multiple point sources of current injection. The solution is obtained with direct explicit matrix inversion techniques. An empirical mixed boundary condition is used at the "infinitely distant" edges of the lower half-space. Accurate solutions using area-discretization method are obtained with significantly less attendant computational costs than with the relaxation, finite-element, or network solution techniques for models of comparable dimensions.

INTRODUCTION

The interpretation of electrical resistivity data has, until recently, been commonly done with the assumption of horizontal layer stratification. The recent developments of data acquisition techniques with high accuracy and substantially higher rates over larger areas warrant a more sophisticated interpretation of the geologic structure. During the last several decades, analytical and analog models have been developed for simulating contacts, dykes, and other simple two and three-dimensional inhomogeneities (Apparao, Roy, and Mallick 1969; Van Nostrand and Cook 1966, McPhar Geophysics 1967, Dey 1967). In most analog modelling, however, only asymptotic behavior for very large conductivity contrasts is considered for a restricted suite of physical dimensions. The resistivity response of inhomogeneities of more general shapes and conductivity have been obtained numerically by Jepsen (1969), Aiken, Hastings, and Sturgul (1973), Coggon (1971) and Madden (1967, 1971). Finite difference evaluation of the response of two-dimensional structures

* Received January 1977.

** Engineering Geoscience and Lawrence Berkeley Laboratory, University of California, Berkeley, California 94720.

due to a point current source was made by Jepsen (1969) and due to a uniform field by Aiken et al. (1973). These techniques solved the problem by using the classical successive-point over-relaxation method due to Southwell (1946). Madden (1967) used a network solution technique to evaluate the potential distribution near a two-dimensional conductivity excited by a point current source. The same problem was solved by Coggon (1971) using a finite element formulation.

In this paper, a direct and explicit finite difference technique is employed to solve for the potential distribution in or on the surface of a half-space with arbitrary two-dimensional distribution of conductivity, due to a point source of excitation. Two dimensional structures defined here are geologic bodies of arbitrary cross-secion with infinite extent along strike. The finite difference scheme is chosen because of the inherent simplicity of the approximation forms which are also easily amenable to Dirichlet, Neumann, or mixed boundary conditions. In contrast to the relaxation techniques, a matrix method is employed to obtain a direct stable solution of the difference equations obtained by approximating Poisson's equation over an irregularly spaced, rectangular grid. The matrix technique has the inherent advantage that the potential distribution in the entire half space under consideration can be found *simultaneously* for multiple source injection points with attendant computational costs that can be 10-50 times less than some of the relaxation techniques hitherto used. As is indicated later, the algorithm developed in this work is also considerably more efficient than finite element and network solution techniques for comparable scales of model simulation in terms of central processor time and core-space required.

Fundamental Relations

Ohm's law relates the current density $\mathbf{J}$ to electric field intensity $\mathbf{E}$ and an isotropic conductivity σ by

$$\mathbf{J} = \sigma\mathbf{E}.$$

Since stationary electric fields are conservative,

$$\mathbf{E} = -\nabla\phi.$$

Hence,

$$\mathbf{J} = -\sigma\nabla\phi.$$

Applying the principle of conservation of charge over a volume, we obtain, using the equation of continuity,

$$\nabla \cdot \mathbf{J} = \frac{\partial\rho}{\partial t}\,\delta(x)\,\delta(y)\,\delta(z), \tag{1}$$

where ρ is the charge density specified at a point in the cartesian x-y-z space by the Dirac delta function.

Equation (1) can be rewritten for a generalized three-dimensional space as

$$-\nabla \cdot [\sigma(x, y, z)\, \nabla\phi(x, y, z)] = \frac{\partial \rho}{\partial t}\, \delta(x_s)\, \delta(y_s)\, \delta(z_s), \tag{2}$$

where (x_s, y_s, z_s) indicate the coordinates of the point source of charge injected in the x-y-z space.

By application of elementary vector calculus, equation (2) can be written as

$$\nabla\sigma(x, y, z) \cdot \nabla\phi(x, y, z) + \sigma(x, y, z)\, \nabla^2\phi(x, y, z) = -\frac{\partial \rho}{\partial t}\, \delta(x_s)\, \delta(y_s)\, \delta(z_s), \tag{3}$$

where

$$\nabla^2 \equiv \frac{\partial^2}{\partial x^2} + \frac{\partial^2}{\partial y^2} + \frac{\partial^2}{\partial z^2}$$

is the Laplacian operator in three dimensions.

If we make the assumption that there be no change in the conductivity distribution in the y (strike) direction, i.e.,

$$\frac{\partial}{\partial y}\, [\sigma(x, y, z)] = 0,$$

equations (2) and (3) can be rewritten as

$$-\nabla \cdot [\sigma(x, z)\, \nabla\phi\, (x, y, z)] = \frac{\partial \rho}{\partial t}\, \delta(x_s)\, \delta(y_s)\, \delta(z_s), \tag{4a}$$

and

$$\nabla\sigma(x, z) \cdot \nabla\phi\, (x, y, z) + \sigma\, (x, z)\, \nabla^2\phi\, (x, y, z) = -\frac{\partial \rho}{\partial t}\, \delta(x_s)\, \delta(y_s)\, \delta(z_s). \tag{4b}$$

Using the vector relation

$$\nabla\sigma \cdot \nabla\phi = \frac{1}{2}\, [-\sigma\nabla^2\phi + \nabla^2(\sigma\phi) - \phi\nabla^2\sigma]$$

and substituting this relation in (4b) we get

$$\nabla^2\{\sigma(x, z)\, \phi\, (x, y, z)\} + \sigma\, (x, z)\, \nabla^2\phi\, (x, y, z) - \phi(x, y, z)\, \nabla^2\sigma(x, z) = -2\, \frac{\partial \rho}{\partial t}\, \delta\, (x_s)\, \delta\, (y_s)\, \delta\, (z_s). \tag{4c}$$

In equations (4a) and (4c), the potential ϕ and the source term $\frac{\partial \rho}{\partial t}\,\delta(x_s)\,\delta(y_s)\,\delta(z_s)$ are functions of x, y, and z and the conductivity σ is a function of x and z. For computational ease, it is preferable to solve these equations in Fourier transformed space (x, K_y, z) by transforming y into the K_y domain. This transformation is performed in the forward and backward direction by the equations

$$\tilde{f}(x, K_y, z) = \int_0^\infty f(x, y, z) \cos(K_y y)\, dy \tag{5a}$$

and

$$f(x, y, z) = \frac{2}{\pi} \int_0^\infty \tilde{f}(x, K_y, z) \cos(K_y y)\, dK_y, \tag{5b}$$

where $f(x, y, z)$ and $\tilde{f}(x, K_y, z)$ are assumed to be even functions of y.

By the transformation (5a) the three-dimensional potential distribution $\phi(x, y, z)$ due to a point source at (x_s, y_s, z_s) over a two-dimensional conductivity distribution $\sigma(x, z)$ is reduced to the two-dimensional transformed potential $\tilde{\phi}(x, K_y, z)$ which is a solution of the transformed equation (4a)

$$-\nabla \cdot [\sigma(x, z)\, \nabla\tilde{\phi}(x, K_y, z)] + K_y^2 \sigma(x, z)\, \tilde{\phi}(x, K_y, z) = \tilde{Q}\delta(x_s)\,\delta(z_s). \tag{6a}$$

Similarly we obtain from (4c)

$$\nabla^2\{\sigma(x, z)\, \tilde{\phi}(x, K_y, z)\} + \sigma(x, z)\, \nabla^2\tilde{\phi}(x, K_y, z) - \tilde{\phi}(x, K_y, z)\, \nabla^2\sigma(x, z) - 2K_y^2\sigma(x, z)\, \tilde{\phi}(x, K_y, z) = -2\tilde{Q}\delta(x_s)\,\delta(z_s) \tag{6b}$$

for a fixed value of K_y. The parameter $\tilde{Q}$ defined in the above equations is the constant steady state current density in (x, K_y, z) space, given by

$$\tilde{Q}\delta(x_s)\,\delta(z_s) = \frac{1}{2}\frac{\partial \rho}{\partial t}\,\delta(x_s)\,\delta(z_s).$$

The current density $\tilde{Q}$ can be related to the current I injected at (x_s, z_s) by

$$\tilde{Q} = \frac{I}{2\Delta A},$$

where ΔA is a representative area in x-z plane about the injection point (x_s, z_s).

The object of this paper is to obtain numerical solutions to equations (6a) and (6b) subject to proper boundary conditions. These boundary conditions are:

(1) $\phi(x, y, z)$ must be continuous across each boundary of the physical property distribution of $\sigma(x, z)$, and

(2) the normal component of $\mathbf{J}\left(\equiv \sigma \frac{\partial \phi}{\partial \eta}\right)$ must also be continuous across each boundary.

The solution of $\tilde{\phi}(x, K_y, z)$ is obtained by deriving the "difference equations" of (6a) or (6b), by proper discretization of the (x, K_y, z) space over which the problem is to be solved. Equation (6a) is amenable to a volume discretization (equivalent to area discretization in x-z space) and equation (6b) is well suited for a point discretization formulation.

Discretization of the Two-Dimensional Resistivity Problem

The generalized form of equations (6a) and (6b) can be written as

$$-\frac{\partial}{\partial x}\left(P(x, z)\frac{\partial \tilde{\phi}}{\partial x}(x, K_y, z)\right) - \frac{\partial}{\partial z}\left(P(x, z)\frac{\partial \tilde{\phi}}{\partial z}(x, K_y, z)\right) + \sigma(x, z)\,\tilde{\phi}(x, K_y, z) = f(x, z);\ (x, z) \in \mathfrak{R} \tag{7}$$

defined in a set $\mathfrak{R}$ which is assumed to be closed and connected, to have a non-void interior and to have a sufficiently regular boundary Γ with outward normal η on which

$$\alpha(x, z)\,\tilde{\phi} + \beta(x, z)\frac{\partial \tilde{\phi}}{\partial \eta} = f_2(x, z);\ (x, z) \in \Gamma. \tag{8}$$

We also have the functions P and f that are at least piecewise continuous in $\mathfrak{R}$ and its closure and which satisfy

$$P(x, z) > 0 \text{ and } \sigma(x, z) > 0;\ (x, z) \in \mathfrak{R}$$

and

$$\alpha(x, z) \geq 0,\ \beta(x, z) \geq 0;$$
$$\alpha + \beta > 0; \quad (x, z) \in \Gamma.$$

Equation (7) is a self-adjoint, strongly connected and nonseparable elliptic equation of second order (Varga 1962). The procedure considered in this paper solves, numerically on a non-uniform rectangular mesh, the problem

$$\mathrm{L}\tilde{\phi} = -\nabla \cdot [\sigma(x, z)\,\nabla\tilde{\phi}] = f(x, z) \text{ on } \mathfrak{R}$$

subject to the boundary conditions (8). The positivity of $\sigma(x, z)$ implies that the operator L is positive definite.

To define the semi-infinite lower half-space with arbitrary conductivity distribution, the set $\mathfrak{R}$ is designed with artificial boundaries simulating *infinitely* distant planes in the horizontal (x-direction) and vertical (z-direction) extent. Such a lower half-space is indicated by the grid shown in figure 1.

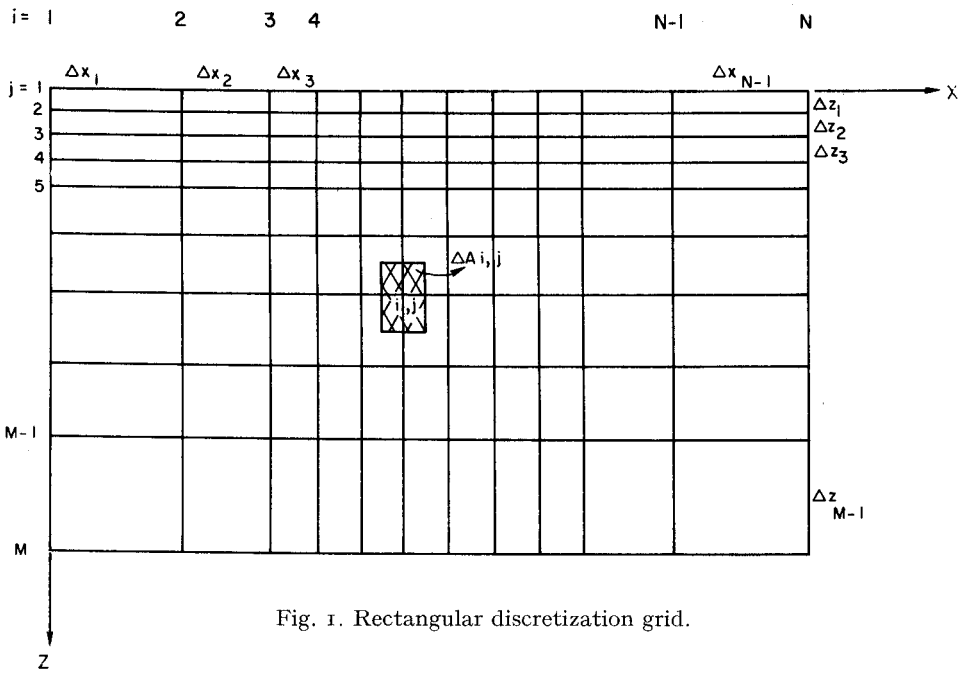

Fig. 1. Rectangular discretization grid.

The grid is chosen to be rectangular with arbitrary, irregular spacing of the nodes in x and z direction, respectively. The nodes in the x-direction are indexed by $i = 1, 2, 3, \ldots, N$, and the nodes in the z-direction are indexed by $j = 1, 2, 3, \ldots, M$. The left and the right infinite edge of the lower half-section are simulated by the lines $i = 1$ and $i = N$, respectively. The bottom edge at infinity is represented by the line $j = M$. The primary potential due to a point source as well as the secondary perturbational potentials due to conductivity inhomogeneities in the lower half space fall inversely with distance in x, y, z space and as $K_0(K_y \cdot r)$ in transform space (where K_0 is the modified Bessel function and r the radial distance). Hence, by a choice of large numbers for M and N with suitably coarsening of the grid as $i \to 1$ and $i \to N$ and $j \to M$, and the application of appropriate boundary conditions, the infinite edges could be simulated by a finite choice of M and N. The representative equations (6a) and (6b) are applied at any node (i, j) to represent an approximation over an area ΔA which is illustrated by the hatched portion in the grid. It can be seen that for a source point in the interior

$$\Delta A = \frac{(\Delta x_i + \Delta x_{i-1}) \cdot (\Delta z_j + \Delta z_{j-1})}{4}$$

and in the limit, at the ground surface with $z \to 0$,

$$\Delta A = \frac{(\Delta x_i + \Delta x_{i-1}) \cdot \Delta z_j}{4}$$

Boundary Conditions Applied on the Edge Γ of the Region $\mathfrak{R}$

Since the simulation of the medium is restricted to the conductive lower half-space alone in $\mathfrak{R}$, it is required that the boundary conditions be specified at points $(x, z) \in \Gamma \cup \mathfrak{R}$. At the ground surface with $z = 0$, this is implemented by applying the Neumann type condition

$$\sigma_{i,j} \frac{\partial \tilde{\phi}_{i,j}}{\partial \eta} = 0, \text{ for all } i = 1, 2, \ldots, N \text{ with } j = 1.$$

The termination of the lower half-plane at $x = \pm \infty$ and $z = \infty$ is done by extending the meshes far enough away from the sources and conductivity inhomogeneities such that the total potential distribution at these edges approaches an asymptotic behavior. The boundary values along these "infinitely" distant edges can be specified from known solutions of the background homogeneous or layered primary distribution of conductivity. Inhomogeneities are viewed as perturbations over this distribution. The boundary conditions along the left, right, and bottom edges thus become Dirichlet-type. In the general case of simulation of more complicated conductivity distributions, often a suitable primary model solution cannot be analytically computed in the (x, K_y, z) space. In such cases, either (i) the potentials at these edges are assumed to be zero (Dirichlet condition) or (ii) at the edges $\partial\tilde{\phi}/\partial\eta$ is assumed to be zero (Neumann condition). It is often found that the first assumption causes an undershoot and the second assumption causes an overshoot in the numerically evaluated potentials at some distance from the point source (Coggon 1971) against the analytical solutions.

We propose to use a mixed boundary condition along the distant left, right, and bottom edges using the asumptotic behavior of ϕ and $\partial\phi/\partial\eta$ expected at large distances from the source. If the observation point along these edges is far enough away from the source points as well as from the conductivity inhomogeneities, the potential $\tilde{\phi}$ in (x, K_y, z) space has the form

$$\tilde{\phi}(x, K_y, z) = AK_0(K_y \cdot r)$$

where K_y is the spatial wave number, r is the radial distance from the source, A a constant and K_0 is the modified Bessel function of order zero.

Hence,

$$\frac{\partial\tilde{\phi}(x, K_y, z)}{\partial\eta} = -AK_yK_1(K_y \cdot r) \cdot \hat{e}_r \cdot \hat{\eta}$$
$$= -AK_yK_1(K_y \cdot r) \cdot \cos\theta,$$

where θ is the angle between the radius vector e_r and the outward normal η.

We can therefore write

$$\frac{\partial\tilde{\phi}(x, K_y, z)}{\partial\eta} + \alpha\tilde{\phi}(x, K_y, z) = 0$$

with

$$\alpha = \frac{K_yK_1(K_y \cdot r)}{K_0(K_y \cdot r)}.$$

Such a mixed boundary condition takes advantage of the physical behavior of the potential at the distant edges and does not require an *a priori* assumption of the nature of the functions ϕ and $\partial\phi/\partial\eta$ that are to be evaluated in terms of primary models. It also has the inherent advantage of reducing the amount of coarsening of the grid required as these edges are approached and the reflections due to virtual sources along the edge nodes are simultaneously eliminated.

In applying this boundary condition the radial distances to all of the edge nodes may be evaluated from the central point on the top-surface of the mesh. While for different source locations the corresponding radial distances are slightly different, in the asymptotic limit used to define α no substantial error arises from this assumption. It is found experimentally that this mixed boundary condition produces a solution for $\tilde{\phi}$ at the edges of the grid that allows a considerably better fit to the analytically computed solution.

Derivation of the Finite Difference Equations

A. *Discretization by Points*

At any node in the set $\mathfrak{N}$, $\tilde{\phi}(x, K_y, z)$ must satisfy (6b)

$$\nabla^2\{\sigma(x, z)\tilde{\phi}(x, K_y, z)\} + \sigma(x, z)\nabla^2\tilde{\phi}(x, K_y, z)$$
$$-\tilde{\phi}(x, K_y, z)\nabla^2\sigma(x, z) - 2K_y^2\sigma(x, z)\tilde{\phi}(x, K_y, z)$$
$$= -2\tilde{Q}\delta(x_s)\delta(z_s).$$

It is seen that the two-dimensional partial differential operator

$$\nabla^2 \equiv \left(\frac{\partial^2}{\partial x^2} + \frac{\partial^2}{\partial z^2}\right)$$

is applied on $\sigma(x, z)$, $\tilde{\phi}(x, K_y, z)$ and $\{\sigma(x, z) \cdot \phi(x, K_y, z)\}$.

The known physical property distribution $\sigma(x, z)$ is discretized at each node by $\sigma_{i,j}$ and in the numerical solution a discrete set $\tilde{\phi}_{i,j}$ at each node is to be evaluated. At any node (i, j) with irregular grid-spacing in x- and z-direction the ∇^2 operator on any distribution of $P_{i,j}$, could be approximated by the finite difference equation as

$$\nabla^2 P_{i,j} = \frac{2}{(\Delta x_i + \Delta x_{i-1})} \cdot \left[\frac{(P_{i-1,j} - P_{ij})}{\Delta x_{i-1}} + \frac{(P_{i+1,j} - P_{i,j})}{\Delta x_i}\right] + \frac{2}{(\Delta z_j + \Delta z_{j-1})} \cdot \left[\frac{(P_{i,j-1} - P_{i,j})}{\Delta z_{j-1}} + \frac{(P_{i,j+1} - P_{i,j})}{\Delta z_j}\right]. \quad (9)$$

The application of the difference operator in equation (9) to equation (6b) for any interior node (i, j) of the grid results in the discretized form given below.

$$\tilde{\phi}_{i-1,j}\left[\frac{-2(\sigma_{i-1,j} + \sigma_{i,j})}{(\Delta x_i + \Delta x_{i-1}) \cdot \Delta x_{i-1}}\right] + \tilde{\phi}_{i+1,j}\left[\frac{-2(\sigma_{i+1,j} + \sigma_{i,j})}{(\Delta x_i + \Delta x_{i-1}) \cdot \Delta x_i}\right] + \tilde{\phi}_{i,j-1}\left[\frac{-2(\sigma_{i,j-1} + \sigma_{i,j})}{(\Delta z_j + \Delta z_{j-1}) \cdot \Delta z_{j-1}}\right] + \tilde{\phi}_{i,j+1}\left[\frac{-2(\sigma_{i,j+1} + \sigma_{i,j})}{(\Delta z_j + \Delta z_{j-1}) \cdot \Delta z_j}\right] + \tilde{\phi}_{i,j}\left[\frac{2(\sigma_{i-1,j} + \sigma_{ij})}{(\Delta x_i + \Delta x_{i-1}) \cdot \Delta x_{i-1}} + \frac{2(\sigma_{i+1,j} + \sigma_{i,j})}{(\Delta x_i + \Delta x_{i-1}) \cdot \Delta x_i} + \frac{2(\sigma_{i,j-1} + \sigma_{i,j})}{(\Delta z_j + \Delta z_{j-1}) \cdot \Delta z_{j-1}} + \frac{2(\sigma_{i,j+1} + \sigma_{i,j})}{(\Delta z_j + \Delta z_{j-1}) \cdot \Delta z_j} + 2K_y^2 \sigma_{i,j}\right] = 2\tilde{Q}\delta(x_s)\,\delta(z_s). \quad (10)$$

In notational form, equation (10) can be written as

$$C_L^{ij}\tilde{\phi}_{i-1,j} + C_R^{ij}\tilde{\phi}_{i+1,j} + C_T^{ij}\tilde{\phi}_{i,j-1} + C_B^{ij}\tilde{\phi}_{i,j+1} + C_P^{ij}\tilde{\phi}_{ij} = 2\tilde{Q}\delta(x_s)\,\delta(z_s), \quad (11)$$

where $$C_L^{ij} = \frac{-2(\sigma_{i-1,j} + \sigma_{i,j})}{(\Delta x_i + \Delta x_{i-1}) \cdot \Delta x_{i-1}}, \quad (11.1)$$

is the coupling coefficient between the nodes (i, j) and $(i - 1, j)$,

$$C_R^{ij} = \frac{-2(\sigma_{i+1,j} + \sigma_{i,j})}{(\Delta x_i + \Delta x_{i-1}) \cdot \Delta x_i}, \quad (11.2)$$

is the coupling coefficient between the nodes (i, j) and $(i + 1, j)$,

$$C_T^{ij} = \frac{-2(\sigma_{i,j-1} + \sigma_{i,j})}{(\Delta z_j + \Delta z_{j-1}) \cdot \Delta z_{j-1}}, \quad (11.3)$$

is the coupling coefficient between the nodes (i, j) and $(i, j - 1)$,

$$C_B^{ij} = \frac{-2(\sigma_{i,j+1} + \sigma_{i,j})}{(\Delta z_j + \Delta z_{j-1}) \cdot \Delta z_j}, \tag{11.4}$$

is the coupling coefficient between the nodes (i, j) and $(i, j+1)$,

and

$$C_P^{ij} = -[C_L^{ij} + C_R^{ij} + C_T^{ij} + C_B^{ij} - 2K_y^2\sigma_{i,j}],$$

is the self coupling at node (i, j).

The difference equation (11) thus obtained indicates that the solution of $\tilde{\phi}$ at node (i, j) is dependent only on the values of $\tilde{\phi}$ at the adjacent nodes $(i-1, j)$, $(i+1, j)$, $(i, j-1)$, and $(i, j+1)$. The coupling coefficients C are functions of the geometry of the discretization grid and the physical property values $\sigma_{i,j}$, and hence known at all nodes in the set $\mathfrak{N}$.

It should be noted that in the finite difference approximation to the operator ∇^2 it is implicitly assumed that the functional distribution of $\tilde{\phi}$, $\sigma\, \partial\tilde{\phi}/\partial x$ and $\sigma\, \partial\tilde{\phi}/\partial z$ are at least piecewise continuous. Equation (11) is valid for any distribution of $\sigma_{i,j} (0 < \sigma < \infty)$ and so, for any interior point in the grid the required boundary conditions on the continuity of $\tilde{\phi}$ and $\sigma\, \partial\tilde{\phi}/\partial\eta$ are satisfied across any of the rectangular element boundaries.

While the coefficients and the self-adjoint form of equation (11) are valid for any interior node, the corresponding equations are somewhat altered for the nodes located at the top surface, and left, right, and bottom edges of the grid. The difference equations (1a)-(8a) for these nodes, with appropriate mixed boundary conditions based on the asymptotic behavior of potentials, are formulated in the appendix A.

B. *Discretization by Area*

At any node in the set $\mathfrak{N}$, the constitutive relation for the unknown potential $\tilde{\phi}(x, K_y, z)$ is given by the self-adjoint eliptic partial differential equation (6a) as

$$-\nabla \cdot [\sigma(x, z)\, \nabla\tilde{\phi}(x, K_y, z)] + K_y^2\sigma(x, z)\, \tilde{\phi}(x, K_y, z) = \tilde{Q}\delta(x_s)\, \delta(z_s) \quad \text{with } (x, z) \in \mathfrak{N}$$

and the boundary condition given by equation (8), such that

$$\beta \frac{\partial\tilde{\phi}}{\partial\eta} = f_2(x, z) - \alpha(x, z)\, \tilde{\phi} \tag{12}$$

with $\alpha \geq 0$, $\beta \geq 0$, and $\alpha + \beta > 0$, prescribed on the boundary $\Gamma \cup \mathfrak{N}$.

The physical property distribution $\sigma_{i,j}$ at any node (i, j) of the rectangular grid, described in the previous section, could be discretized in the sense that $\sigma_{i,j}$ now indicates the conductivity in a region bounded by the nodes (i, j) and $(i + 1, j)$ in the x-direction and the nodes $(i, j + 1)$ and $(i + 1, j + 1)$ in the z-direction. The numerical solution of (6a) that consists of a discretized set of $\tilde{\phi}_{i,j}$ at each node, is to be evaluated. As in the previous section, the node (i, j) is assumed to represent the closed mesh region $\Delta A_{i,j}$ about the node, as illustrated in figure 1. It is seen that for a nodal point in the interior one has

$$\Delta A_{i,j} = \frac{(\Delta x_i + \Delta x_{i-1})\ (\Delta z_j + \Delta z_{j-1})}{4}$$

and the limit $z \to 0$, — a nodal point on the ground surface —

$$\Delta A_{i,j} = \frac{(\Delta X_i + \Delta x_{i-1})\ .\ \Delta z_j}{4}.$$

For each node (i, j) for which $\tilde{\phi}_{i,j}$ is unknown, we now integrate equation (6a) over the corresponding mesh region $\Delta A_{i,j}$ to obtain

$$-\iint_{\Delta A_{i,j}} \nabla\ .\ \{\sigma(x_i z_j)\ \nabla\tilde{\phi}\ (x_i, K_y, z_j)\}\ \mathrm{d}x_i \mathrm{d}z_j$$

$$+\iint_{\Delta A_{i,j}} K_y^2 \sigma(x_i, z_j)\ \tilde{\phi}(x_i, K_y, z_j)\ \mathrm{d}x_i \mathrm{d}z_j$$

$$= \iint_{\Delta A_{i,j}} \tilde{Q}\delta(x_s)\ \delta(z_s)\ \mathrm{d}x_i \mathrm{d}z_j.$$

Using the relation $\tilde{Q} = \dfrac{I}{2\Delta A_{i,j}}$

$$-\iint_{\Delta A_{i,j}} \nabla\ .\ \{\sigma(x_i, z_j)\ \nabla\tilde{\phi}(x_i, K_y, z_j)\}\ \mathrm{d}x_i \mathrm{d}z_j$$

$$+\iint_{\Delta A_{i,j}} K_y^2 \sigma(x_i, z_j)\ \tilde{\phi}(x_i, K_y, z_j)\ \mathrm{d}x_i \mathrm{d}z_j$$

$$= \frac{I}{2}\ \delta(x_s)\ \delta(z_s). \tag{13}$$

Using Green's theorem we obtain

$$\iint_{\Delta A_{i,j}} \nabla\ .\ (\sigma\nabla\tilde{\phi})\ \mathrm{d}a = \oint_{L_{i,j}} \sigma\ \frac{\partial\tilde{\phi}}{\partial\eta}\ \mathrm{d}l, \tag{14}$$

where η is the outward normal direction and $L_{i,j}$ is the contour line enclosing the mesh region $\Delta A_{i,j}$. It is seen from equation (14) that over every element of $\mathfrak{R}$ and on the boundary Γ the boundary conditions given by equation (12) could be directly implemented in the first term of the discretized equation (13).

The detailed description of the distribution of $\sigma_{i,j}$, the representative mesh area $\Delta A_{i,j}$, and the line contour $L_{i,j}$ about a node (i, j) in the interior of the grid is illustrated in figure 2. The first term on the left hand node of equation (12) is given by

$$-\iint_{\Delta A_{i,j}} \nabla \cdot (\sigma_{i,j} \nabla \tilde{\phi}_{i,j})\, dx_i dz_j = -\oint_{L_{ij}} \sigma_{ij} \frac{\partial \tilde{\phi}_{i,j}}{\partial \eta}\, dl. \tag{15}$$

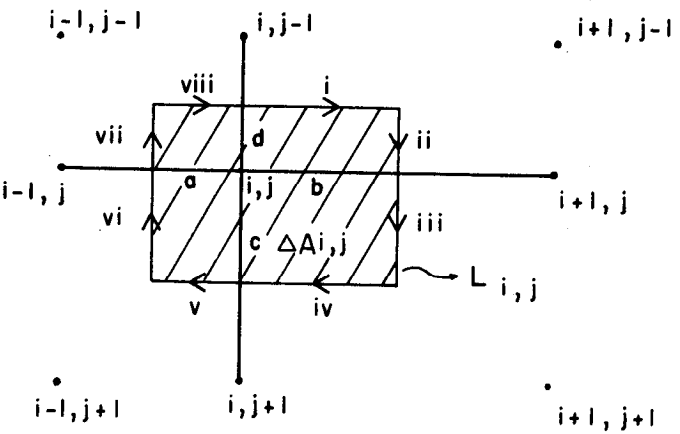

Fig. 2. Discretized area element $\Delta A_{i,j}$.

The contour integration along the line $L_{i,j}$ is subdivided into eight subsections as indicated in figure 2. Integrating along the entire path L_{ij} we get by approximating $\partial\tilde{\phi}/\partial\eta$ by central difference

$$\oint_{L_{i,j}} \sigma_{i,j} \cdot \frac{\partial \tilde{\phi}_{i,j}}{\partial \eta}\, dl = \frac{\Delta x_i\, \sigma_{i,j-1}}{2} \left(\frac{\tilde{\phi}_{i,j-1} - \tilde{\phi}_{i,j}}{\Delta z_{j-1}} \right)$$

$$+ \frac{\Delta z_{j-1}\, \sigma_{i,j-1}}{2} \cdot \left(\frac{\tilde{\phi}_{i+1,j} - \tilde{\phi}_{i,j}}{\Delta x_i} \right)$$

$$+ \frac{\Delta z_j \cdot \sigma_{i,j}}{2} \left(\frac{\tilde{\phi}_{i+1,j} - \tilde{\phi}_{i,j}}{\Delta x_i} \right) + \frac{\Delta x_i \cdot \sigma_{i,j}}{2}$$

$$\cdot \left(\frac{\tilde{\phi}_{i-1,j-1} - \tilde{\phi}_{i,j}}{\Delta z_j} \right) + \frac{\Delta x_{i-1} \cdot \sigma_{i-1,j}}{2}$$

$$\cdot \left(\frac{\tilde{\phi}_{i-1,j-1} - \tilde{\phi}_{i,j}}{\Delta z_j}\right) + \frac{\Delta z_j \cdot \sigma_{i-1,j}}{2}$$
$$\cdot \left(\frac{\tilde{\phi}_{i-1,j} - \tilde{\phi}_{i,j}}{\Delta x_{i-1}}\right) + \frac{\Delta z_{i-1} \cdot \sigma_{i-1,j-1}}{2}$$
$$\left(\frac{\tilde{\phi}_{i-1,j} - \tilde{\phi}_{i,j}}{\Delta x_{i-1}}\right) + \frac{\Delta x_{i-1} \cdot \sigma_{i-1,j-1}}{2}$$
$$\left(\frac{\tilde{\phi}_{i,j-1} - \tilde{\phi}_{i,j}}{\Delta z_{j-1}}\right). \tag{16}$$

Similarly, the second term on the left hand side of equation (12) can be expanded as

$$\iint_{\Delta A_{i,j}} K_y^2 \, \sigma_{i,j} \, \tilde{\phi}_{i,j} \, dx_i \, dz_j = K_y^2 \, \tilde{\phi}_{i,j}$$
$$\left[\frac{\sigma_{i-1,j-1} \cdot \Delta x_{i-1} \cdot \Delta z_{j-1}}{4} + \frac{\sigma_{i,j-1} \cdot \Delta x_i \cdot \Delta z_{j-1}}{4}\right.$$
$$\left. + \frac{\sigma_{i,j} \cdot \Delta x_i \cdot \Delta z_j}{4} + \frac{\sigma_{i-1,j} \cdot \Delta x_{i-1} \cdot \Delta z_j}{4}\right] \equiv A(\sigma_{i,j}, A_{i,j}) \cdot \tilde{\phi}_{i,j}. \tag{17}$$

Substituting the difference approximation (16) and (17) in equation (13), we obtain for an interior node point (i, j)

$$C_L^{ij} \cdot \tilde{\phi}_{i-1,j} + C_R^{ij} \cdot \tilde{\phi}_{i+1,j} + C_{ij}^T \cdot \phi_{i,j-1}$$
$$+ C_B^{ij} \cdot \phi_{i,j+1} + C_P^{ij} \cdot \phi_{i,j} = \frac{I}{2} \delta(x_s) \, \delta(z_s), \tag{18}$$

where $C_L^{ij} = -\left[\dfrac{\Delta z_{j-1} \cdot \sigma_{i-1,j-1} + \Delta z_j \sigma_{i-1,j}}{2\Delta x_{i-1}}\right]$ (18.1)

is the coupling coefficient between nodes (i, j) and $(i - 1, j)$,

$$C_R^{ij} = -\left[\frac{\Delta z_{j-1} \cdot \sigma_{i,j-1} + \Delta z_j \cdot \sigma_{i,j}}{2\Delta x_i}\right] \tag{18.2}$$

is the coupling coefficient between the nodes (i, j) and $(i + 1, j)$,

$$C_T^{ij} = -\left[\frac{\Delta x_{i-1} \cdot \sigma_{i-1,j-1} + \Delta x_i \cdot \sigma_{i,j-1}}{2\Delta z_{j-1}]}\right] \tag{18.3}$$

is the coupling coefficient between the nodes (i, j) and $(i, j - 1)$,

$$C_B^{ij} = -\left[\frac{\Delta x_{i-1} \cdot \sigma_{i-1,j} + \Delta x_i \cdot \sigma_{i,j}}{2\Delta z_j}\right] \tag{18.4}$$

is the coupling coefficient between the nodes (i, j) and $(i, j+1)$,

and

$$C_{ij}^P = -\left[C_L^{ij} + C_R^{ij} + C_T^{ij} + C_B^{ij} - A(\sigma_{i,j} A_{i,j})\right] \tag{18.5}$$

is the self coupling coefficient at node (i, j).

The self-adjoint difference equation (18) indicates that the solution of $\tilde{\phi}$ at (i, j) node is dependent only on the values of $\tilde{\phi}$ at the adjacent nodes $(i-1, j)$, $(i+1, j)$, $(i, j-1)$ and $(i, j+1)$. The coupling coefficients are known functions of the geometry and the physical property distribution in the set $\mathfrak{R}$.

The application of the boundary conditions on Γ is made such that on the ground surface $(z = 0)$, the equation (12) has $\alpha = 0$, $\beta = \sigma_{i,j}$, and $f_2 = 0.0$. On the left, right, and lower edge of Γ, simulating the "infinitely" distant boundaries, equation (12) is applied with $\alpha = K_y K_1(K_y \cdot r)/K_0(K_y \cdot r)$, $\beta = 1$, $f_2 = 0.0$. The modified difference equations (1b)-(8b) obtained upon application of these conditions at the special nodal points, are developed in appendix B.

Equations (11) and (1a)-(8a) obtained with the discretization by points or the set of equations (18) and (1b)-(8b) obtained through discretization by area, can be solved for all $\tilde{\phi}_{i,j}$ by using Successive Point Overrelaxation (Southwell 1946), Successive Line Overrelaxation (Varga 1962), Alternating Direction Iterative Methods (Peaceman and Rachford 1955, Douglas and Rachford 1956, and Gunn 1964). In these methods, an initial assumed distribution of $\tilde{\phi}_{i,j}$ over the grid is relaxed by successive refinement through iterations. The refinements in the individual methods are either in terms of individual nodes, successive rows or columns of nodes or of $\tilde{\phi}_{i,j}$ alternately along a column and a row. The refinement obtained upon an iteration is further updated by the use of an optimal overrelaxation factor or by successive use of the Chebychev overrelaxation acceleration parameter (Concus and Golub 1973). In the large grids under consideration (1000-2000 nodal points), these techniques require a minimum of 30-100 iteration sweeps through the entire grid for each location of the point source of current injection. In addition, the convergence rates of these iterative techniques are highly dependent on the dimensions of the grid spacings and the nature of the physical property distribution. Detailed analysis of these techniques and their comparison are given by Varga (1962), Forsythe and Wasow (1960), and Mitchell (1969). It is found experimentally that for the nonseparable, elliptic, self-adjoint difference equations that occur in the present formulation, direct matrix inversion techniques can be applied to solve for potential distributions with multiple point source locations, with

an attendant cost of computation that could be 10 to 50 times less than the iterative techniques mentioned above.

Matrix Formulation

In the matrix formulation, equations (11) and (1a)-(8a) or the set of equations (18) and (1b)-(8b) applied to all nodes (i, j), $i = 1, 2, \ldots, N$ and $j = 1, 2, \ldots, M$ may be solved simultaneously. For an example, a 4×4 grid is shown in figure 3.

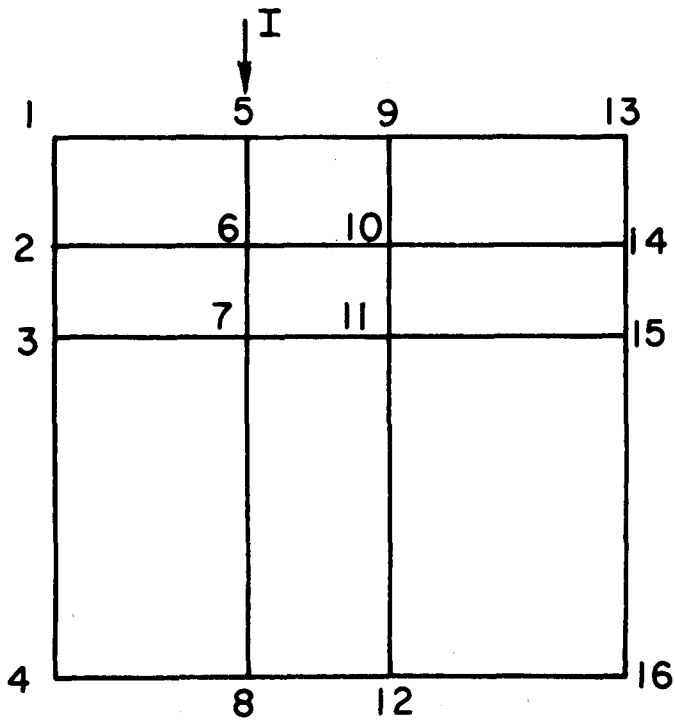

Fig. 3. Sample node numbering convention for rectangular grid.

The individual nodes are numbered 1 through 16 starting from the left topcorner and periodically increasing along each column. The set of simultaneous equations for all the nodes in the grid can be written in matrix form (see table 1) or, symbolically, as

$$\mathbf{C}\tilde{\phi} = \mathbf{S}. \tag{19}$$

The $MN \times MN$ matrix $\mathbf{C}$ is called the Capacitance Matrix and is a function of the geometry and the physical property distribution in the grid. It is to be noted that for multiple source locations, the matrix $\mathbf{C}$ remains unaltered.

TABLE I

Explicit form of the equation $\mathbf{C}\,\tilde{\phi} = \mathbf{S}$

$$
\begin{bmatrix}
C_P(1) & C_B(1) & 0 & 0 & C_R(1) & 0 & 0 & 0 & 0 & 0 & 0 & 0 & 0 & 0 & 0 & 0 \\
C_T(2) & C_P(2) & C_B(2) & 0 & 0 & C_R(2) & 0 & 0 & 0 & 0 & 0 & 0 & 0 & 0 & 0 & 0 \\
0 & C_T(3) & C_P(3) & C_B(3) & 0 & 0 & C_R(3) & 0 & 0 & 0 & 0 & 0 & 0 & 0 & 0 & 0 \\
0 & 0 & C_T(4) & C_P(4) & 0 & 0 & 0 & C_R(4) & 0 & 0 & 0 & 0 & 0 & 0 & 0 & 0 \\
C_L(5) & 0 & 0 & 0 & C_P(5) & C_B(5) & 0 & 0 & C_R(5) & 0 & 0 & 0 & 0 & 0 & 0 & 0 \\
0 & C_L(6) & 0 & 0 & C_T(6) & C_P(6) & C_B(6) & 0 & 0 & C_R(6) & 0 & 0 & 0 & 0 & 0 & 0 \\
0 & 0 & C_L(7) & 0 & 0 & C_T(7) & C_P(7) & C_B(7) & 0 & 0 & C_R(7) & 0 & 0 & 0 & 0 & 0 \\
0 & 0 & 0 & C_L(8) & 0 & 0 & C_T(8) & C_P(8) & 0 & 0 & 0 & C_R(8) & 0 & 0 & 0 & 0 \\
0 & 0 & 0 & 0 & C_L(9) & 0 & 0 & 0 & C_P(9) & C_B(9) & 0 & 0 & C_R(9) & 0 & 0 & 0 \\
0 & 0 & 0 & 0 & 0 & C_L(10) & 0 & 0 & C_T(10) & C_P(10) & C_P(10) & 0 & 0 & C_R(10) & 0 & 0 \\
0 & 0 & 0 & 0 & 0 & 0 & C_L(11) & 0 & 0 & C_T(11) & C_P(11) & C_B(11) & 0 & 0 & C_R(10) & 0 \\
0 & 0 & 0 & 0 & 0 & 0 & 0 & C_L(12) & 0 & 0 & C_T(12) & C_P(12) & 0 & 0 & 0 & C_R(12) \\
0 & 0 & 0 & 0 & 0 & 0 & 0 & 0 & C_L(13) & 0 & 0 & 0 & C_P(13) & C_P(13) & 0 & 0 \\
0 & 0 & 0 & 0 & 0 & 0 & 0 & 0 & 0 & C_L(14) & 0 & 0 & C_T(14) & C_P(14) & C_B(14) & 0 \\
0 & 0 & 0 & 0 & 0 & 0 & 0 & 0 & 0 & 0 & C_L(15) & 0 & 0 & C_T(15) & C_P(15) & C_B(15) \\
0 & 0 & 0 & 0 & 0 & 0 & 0 & 0 & 0 & 0 & 0 & C_L(16) & 0 & 0 & C_T(16) & C_P(16)
\end{bmatrix}
\begin{bmatrix} \tilde{\phi}_1 \\ \tilde{\phi}_2 \\ \tilde{\phi}_3 \\ \tilde{\phi}_4 \\ \tilde{\phi}_5 \\ \tilde{\phi}_6 \\ \tilde{\phi}_7 \\ \tilde{\phi}_8 \\ \tilde{\phi}_9 \\ \tilde{\phi}_{10} \\ \tilde{\phi}_{11} \\ \tilde{\phi}_{12} \\ \tilde{\phi}_{13} \\ \tilde{\phi}_{14} \\ \tilde{\phi}_{15} \\ \tilde{\phi}_{16} \end{bmatrix}
=
\begin{bmatrix} 0 \\ 0 \\ 0 \\ 0 \\ S_5 \\ 0 \\ 0 \\ 0 \\ 0 \\ 0 \\ 0 \\ 0 \\ 0 \\ 0 \\ 0 \\ 0 \end{bmatrix}
$$

Hence, only one inversion of **C** provides the solution to different sets of vectors $\tilde{\phi}$ for the different source locations that constitute the vector **S**, through back substitution. This is an inherent advantage in the direct matrix solution method over the semi-explicit iterative methods mentioned previously.

The structure of the matrix **C** is blocktridiagonal, sparse, and banded. The choice of sequential numbering of nodes along columns or rows dictates the bandwidth required. In resistivity surveying with large surface coverage a grid with $N \gg M$ is usually required. The numbering of nodes along rows causes the number of co-diagonals to be $2N$; if the nodes were to be numbered along columns, as shown in figure 3, the number of co-diagonals would be $2M$ resulting in considerable saving of the core space required in the solution technique.

The coefficients in the matrix **C** as indicated in equation (19) are derived by using the mixed boundary condition along the "infinitely distant" edges of the mesh in x- and z-directions. If, however, for nodes lying on the left, right, and bottom edges (i.e., 1-4, 13-16, and 8 and 12, respectively) known potential values (e.g. primary model potentials) are to be assigned (Dirichlet condition), this could be simply achieved by making the corresponding row $C_{i,j} = \delta_{ij}$ and by adding to the corresponding element in the vector **S** the known Dirichlet potential for the node.

The capacitance matrix **C** has the following properties.

(*i*) $C_{i,i} > 0, i = 1, 2, \ldots, MN;$

(*ii*) $C_{i,i} \geq \sum_{\substack{j=1 \\ j \neq i}}^{MN} | C_{i,j} |, i = 1, 2, \ldots, MN,$

i.e. C is diagonally dominant;

(*iii*) C is irreducible and has a strongly connected directed graph (Varga 1962); and

(*iv*) C possess Young's Property A (Young 1954).

It is shown by Varga (1962) that the explicit difference equations that give rise to the matrix **C** with properties described above are inherently stable for arbitrary grid spacings.

The matrix **C** when obtained through discretization by point representation is found to be nonsymmetric, for unequal grid spacings in $\pm x$- and $\pm z$-direction and for arbitrary distribution of $\sigma(x, z)$. Discretization by area over an inequally spaced rectangular grid with arbitrary distribution of $\sigma(x, z)$ as indicated by equations (12) and (1b)-(8b), however, makes the capacitance matrix **C** a positive definite, symmetric matrix.

The solution of the equation $\mathbf{C}\tilde{\phi} = \mathbf{S}$, when $\mathbf{C}$ is nonsymmetric and banded, is best done by the well known Gaussian elimination algorithm. For the area discretization method, when $\mathbf{C}$ is symmetric and positive definite, the solution is best obtained by symmetric Cholesky decomposition (Martin and Wilkinson 1965). This method is based on the following theorem:

If $\mathbf{A}$ is a positive definite matrix of order n and banded form such that

$$a_{ij} = 0 \; (|\, i - j \,| > m),$$

then there exists a real, nonsingular lower triangular matrix $\mathbf{L}$ such that

$$\mathbf{L}\mathbf{L}^T = \mathbf{A} \text{ where } L_{ij} = 0(i - j > m). \tag{20}$$

The elements of $\mathbf{L}$ may be determined row by row by equating elements on both sides of equation (20). The solution of the set of equations $\mathbf{A}\mathbf{x} = \mathbf{b}$ can be determined in the steps

$$\mathbf{L}\mathbf{y} = \mathbf{b}; \; \mathbf{L}^T\mathbf{x} = \mathbf{y}. \tag{21}$$

This decomposition technique is especially effective when $m \ll n$. There are then approximately $n(m + 1)\,(m + 2)/2$ multiplication and n square roots in the decomposition, approximately $2n(m + 1)$ multiplications are involved in the solution steps, and any number of right hand sides can be processed when $\mathbf{L}$ is known. For symmetric, banded matrices, this operation count is lower than that for Gaussian elimination methods.

Inverse Transformation of $\tilde{\phi}(x, K_y, z)$

The solution of $\tilde{\phi}(x, K_y, z)$ is outlined in the previous sections. In order to obtain the solution of ϕ in the (x, y, z) domain, the set of $\tilde{\phi}(x, K_y, z)$ for several optimal values of K_y, chosen to discretize the interval $0 < K_y < \infty$, are obtained. The inverse Fourier transform is then performed by numerically integrating equation (5b). The general behavior of $\tilde{\phi}(x, K_y, z)$ indicates an asymptotically flat response as $K_y \to 0$ and a monotonic fall off to zero as $K_y \to \infty$. The integration is performed by fitting the envelope of $\tilde{\phi}(K_y)$ in each subsection $K_{y1} \leq K_y \leq K_{y2}$ by an exponential and using the analytic form

$$\int_{K_{y_1}}^{K_{y_2}} e^{-aK_y} \cos(K_y b)\, dK_y = \frac{e^{-aKy}}{a^2 + b^2} \cdot [b \sin(bK_y) - a \cos(bK_y)] \Big|_{K_{y_1}}^{K_{y_2}}$$

and taking the cumulative sum of these subsectional integrals up to reasonably large values of K_y to obtain an accuracy of 1 percent.

Determination of the Apparent Resistivity Response of 2-Dimensional Structures

In electrical resistivity surveys a current source $+ I$ and a current sink $- I$ are used to energize the conductive earth. A potential difference ΔV is measured between two points located at arbitrary azimuthal orientation (for surface arrays) or colatitudinal configuration (as in down-hole-surface arrays). A parameter *apparent resistivity* is defined as a function

$$\rho_a = G \frac{\Delta V}{I} \tag{22}$$

where, for the configuration illustrated in figure 4,

$$G = 2\pi \frac{\mathrm{I}}{\left(\frac{\mathrm{I}}{r_1} - \frac{\mathrm{I}}{r_2} - \frac{\mathrm{I}}{r_3} + \frac{\mathrm{I}}{r_4}\right)}.$$

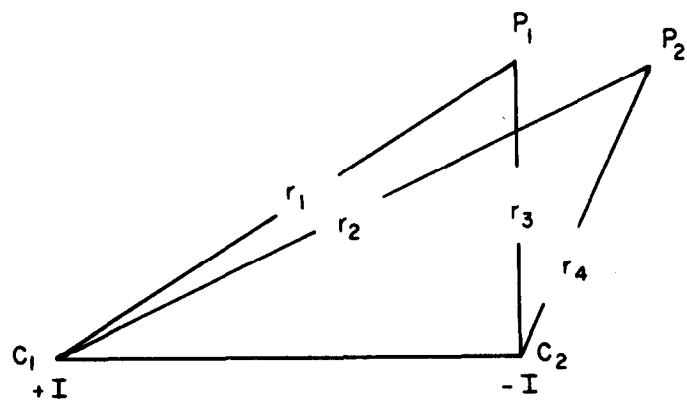

Fig. 4. Electrode configuration for an arbitrary geometric factor.

For a homogeneous half-space, ρ_a is the true intrinsic resistivity of the medium. If, however, the lower semi-infinite medium has inhomogeneous conductivity distribution, ρ_a indicates the resistivity of an apparent homogeneous half-space that results in an identical ΔV for the transmitter-receiver array under consideration. All interpretations of electrical resistivity work are done using the apparent resistivity concept described above.

It can be seen that the d.c. potential distribution at any point is a superposition of the solutions of two point sources of current located at the transmitting electrodes of amplitude $+ I$ and $- I$.

Results

To estimate the accuracy of the two-dimensional resistivity technique described in the previous sections, a two-layered earth model was simulated.

The resistivity of the top layer of thickness 1000 m was assumed to be 100 Ωm and that of the bottom layer to be 10 Ωm. A collinear dipole-dipole array was deployed in a sounding mode with a dipole length of 1000 m and with dipole separations $N = 1, 2, \ldots, 15$. The results of such a numerical simulation are indicated in figure 5 with circles, and the analytically computed response for the two layered model is shown by the curve with solid line. It can be seen that the numerical results approach the analytic solution with an accuracy of better than 5%.

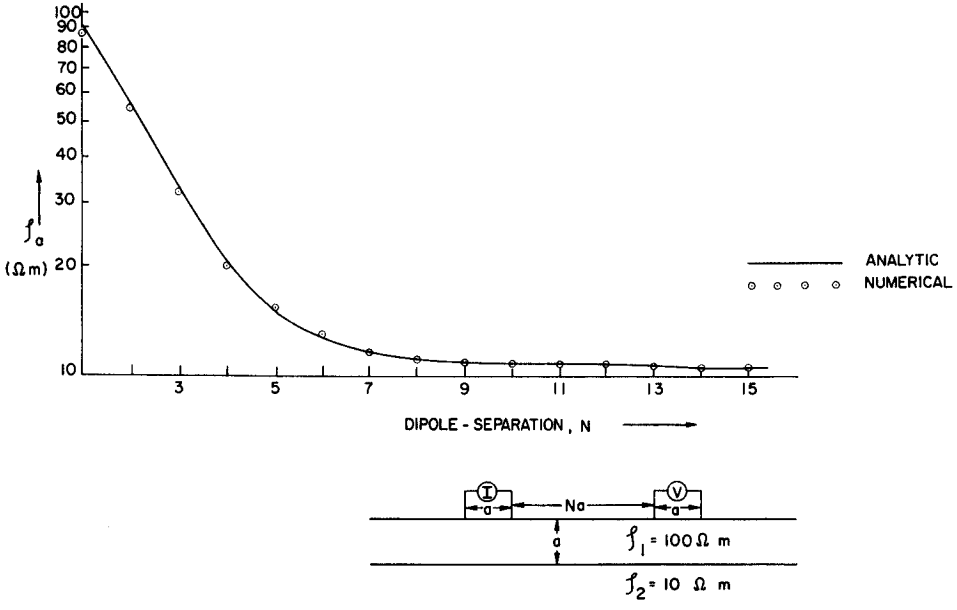

Fig. 5. Comparison of numerical and analytic results for a dipole dipole sounding over a two-layer model.

The rectangular grid used in the simulation of the above model consisted of 113 nodes in the x-direction and 16 nodes in the z-direction. The central 103 nodes were equally spaced and finely described. The node spacing approaching the left and the right edge were rapidly coarsened to simulate the infinitely distant edges. The vertical resolution of the node distribution was similarly fine near the ground surface and coarsened considerably to approach the "infinite depth" boundary. In the result presented, the discretization by area method was employed with the empirical mixed-boundary condition applied at the edges.

In another example, illustrated in figure 6, a routine interpretation over a complex structure is done by obtaining a "best fit" to the apparent resistivity data observed in field survey, using the collinear dipole-dipole array, displayed in a standard pseudo-section plot.

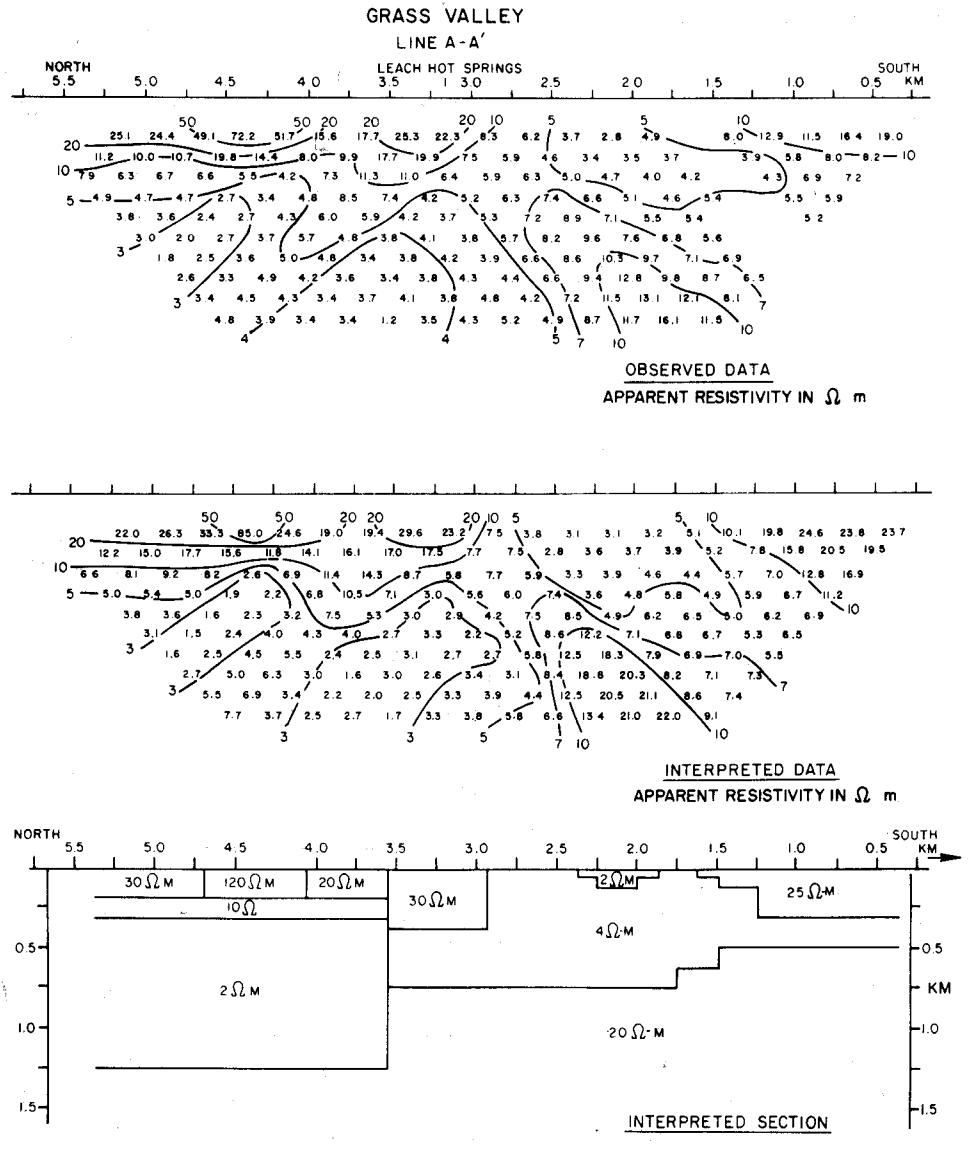

Fig. 6. Interpretation of an apparent resistivity pseudo section.

Discussion

In most of the standardized use in our interpretational task for a collinear dipole-dipole array, a grid of 113 × 16 (= 1808) nodes is used. The solution at each of these 1808 nodes is obtained for 23 transmitting point sources. The discretized problem is solved in our algorithm by obtaining repeated sets of

solution obtained for five optimally chosen K_y values. The CP-times required to solve for an arbitrary 2-dimensional structure are 41 seconds and 24 seconds for discretization by point and discretization by area methods, respectively, on a CDC 7600 machine. An identical problem when solved using a network solution technique to the same accuracy requires about 35 seconds of CP-time using comparable core storage. A finite element algorithm available to us could not be compared for an equivalent extent of the pseudo section evaluation, due to lack of core space to fit the problem. However, from comparison of problems of smaller dimensions, the new technique is estimated to be considerably faster and more economic in terms of cost and storage requirements than the finite element algorithm (Coggon 1971).

ACKNOWLEDGEMENTS

The authors are indebted to Mike Hoversten for computational assistance. Support for this work has been provided by the United States Energy Research and Development Administration through Lawrence Berkeley Laboratory.

APPENDIX A

DIFFERENCE EQUATIONS FOR THE BOUNDARY NODES USING POINT DISCRETIZATION SCHEME

a. *For nodes located on the line* $z = 0$

For all nodes (i, j) with $i = 2, 3, \ldots, N - 1, j = 1$, the boundary condition is of the Neumann type, i.e.

$$\sigma \left.\frac{\partial \tilde{\phi}}{\partial \eta}\right|_{z=0} = 0.$$

This is implemented by assuming a fictitious row of nodes in the air at $j = 0$, such that the potential $\phi_{i,2}$ and conductivity $\sigma_{i,2}$ at nodes $(i, 2)$ are reflected at the imaginary nodes $(i, 0)$. This assumption leads to the difference form of equation (6b) given by

$$C_L^{ij}\,\tilde{\phi}_{i-1,j} + C_R^{ij}\,\tilde{\phi}_{i+1,j} + C_B^{ij}\,\tilde{\phi}_{i,j+1} + C_P^{ij}\,\tilde{\phi}_{i,j} = 2\tilde{Q}\delta(x_s)\,\delta(z_s), \tag{1a}$$

where the coupling coefficients are given by

$$C_L^{ij} = \frac{-2(\sigma_{i-1,j} + \sigma_{i,j})}{(\Delta x_i + \Delta x_{i-1}) \cdot \Delta x_{i-1}}, \tag{1.1a}$$

$$C_R^{ij} = \frac{-2(\sigma_{i+1,j} + \sigma_{i,j})}{(\Delta x_i + \Delta x_{i-1}) \cdot \Delta x_i}, \tag{1.2a}$$

$$C_B^{ij} = \frac{-2(\sigma_{i,j+1} + \sigma_{i,j})}{(\Delta z_j)^2}, \tag{1.3a}$$

and

$$C_P^{ij} = -[C_L^{ij} + C_R^{ij} + C_B^{ij} - 2K_y^2\sigma_{i,j}]. \tag{1.4a}$$

b. *For the top, left, and right corner nodes on line* $z = 0$

The nodes $(1, 1)$ and $(N, 1)$ which lie on the "infinite" boundary, the normal component of **J** in z-direction is zero (Neumann condition). The x-component of **J**, however, satisfies the mixed boundary condition

$$\frac{\partial\tilde{\phi}}{\partial x} + \alpha\tilde{\phi}\cos\theta = 0 \quad \text{with } \alpha = \frac{K_y K_1(K_y r)}{K_0(K_y r)},$$

where θ is the angle between the radius vector r from the source point and the outward normal in x-direction. If we assume a set of fictitious column of nodes in the lower half-space at $i = 0$ and $i = N + 1$, then the potential at these nodes could be expressed entirely in terms of the potential on the boundary node (i, j) through the mixed boundary condition.

These conditions applied to the equation (6b) result in the difference equations, for the top left node $(1, 1)$:

$$C_R^{ij}\tilde{\phi}_{i+1,j} + C_B^{ij}\tilde{\phi}_{i,j+1} + C_P^{ij}\tilde{\phi}_{ij} = 2Q\delta(x_s)\,\delta(z_s), \tag{2a}$$

where

$$C_R^{ij} = \frac{-(\sigma_{i,j} + \sigma_{i+1,j})}{(\Delta x_i)^2}, \tag{2.1a}$$

$$C_B^{ij} = \frac{-2(\sigma_{i,j+1} + \sigma_{i,j})}{(\Delta z_j)^2},$$

$$C_P^{ij} = -[C_R^{ij} + C_B^{ij} - 2K_y^2\sigma_{i,j}] - \frac{2\sigma_{i,j}}{(\Delta x_i)^2}(1 - \alpha\Delta x_i\cos\theta), \tag{2.3a}$$

and for the top right node $(N, 1)$:

$$C_L^{ij}\tilde{\phi}_{i-1,j} + C_B^{ij}\tilde{\phi}_{i,j+1} + C_P^{ij}\tilde{\phi}_{i,j} = 2\tilde{Q}\delta(x_s)\,\delta(z_s), \tag{3a}$$

where

$$C_L^{ij} = \frac{-(\sigma_{i-1,j} + \sigma_{i,j})}{(\Delta x_{i-1})^2}, \tag{3.1a}$$

$$C_B^{ij} = \frac{-2(\sigma_{i,j+1} + \sigma_{i,j})}{(\Delta z_j)^2}, \tag{3.2a}$$

and

$$C_P^{ij} = -[C_L^{ij} + C_B^{ij} - 2K_y^2\sigma_{i,j}] - \frac{2\sigma_{i,j}}{(\Delta x_{i-1})^2}(1 - \alpha\Delta x_{i-1}\cos\theta). \tag{3.3a}$$

c. *For the nodes located on the bottom edge of the mesh* ($z \to \infty$)

At the nodes (i, M), $i = 2, 3, \ldots, N-1$, that are on the lower "infinite" boundary, the application of the mixed boundary condition described above results in the difference equation

$$C_L^{ij}\,\tilde{\phi}_{i-1,j} + C_R^{ij}\,\tilde{\phi}_{i+1,j} + C_T^{ij}\,\tilde{\phi}_{i,1-j} + C_P^{ij}\,\tilde{\phi}_{i,j} = 2\tilde{Q}\delta(x_s)\,\delta(z_s) \tag{4a}$$

with the coupling coefficients

$$C_L^{ij} = \frac{-2(\sigma_{i-1,j} + \sigma_{i,j})}{(\Delta x_i + \Delta x_{i-1}) \,.\, \Delta x_{i-1}}, \tag{4.1a}$$

$$C_R^{ij} = \frac{-2(\sigma_{i+1,j} + \sigma_{i,j})}{(\Delta x_i + \Delta x_{i-1}) \,.\, \Delta x_i}, \tag{4.2a}$$

$$C_T^{ij} = \frac{-(\sigma_{i,j-1} + \sigma_{i,j})}{(\Delta z_{j-1})^2}, \tag{4.3a}$$

and

$$C_T^{ij} = -[C_L^{ij} + C_R^{ij} + C_T^{ij} - 2K_y^2\sigma_{i,j}] - \frac{2\sigma_{i,j}}{(\Delta z_{j-1})^2} \,.\, (1 - \alpha\Delta z_{i-1} \,.\, \cos\theta). \tag{4.4a}$$

d. *For the bottom left and right corner nodes*

For the nodes $(1, M)$ and (N, M) the components of J_x and J_z satisfy the mixed boundary conditions

$$\frac{\partial\tilde{\phi}}{\partial x} + \alpha\,\tilde{\phi}\cos\theta_1 = 0$$

and

$$\frac{\partial\tilde{\phi}}{\partial z} + \alpha\,\tilde{\phi}\cos\theta_2 = 0,$$

where θ_1 and θ_2 are the angles between the radial distance r from the source to the node (i, j) and the outward normals in the x- and z-directions, respectively.

The application of these boundary conditions results in the difference equation for the node $(1, M)$ given below:

$$C_R^{ij}\,\tilde{\phi}_{i+1,j} + C_T^{ij}\,\tilde{\phi}_{i,j-1} + C_P^{ij}\,\tilde{\phi}_{i,j} = 2\tilde{Q}\delta(x_s)\,\delta(z_s), \tag{5a}$$

where

$$C_R^{ij} = -\frac{(\sigma_{i+1,j} + \sigma_{i,j})}{(\Delta x_i)^2} \tag{5.1a}$$

$$C_T^{ij} = -\frac{(\sigma_{i,j-1} + \sigma_{i,j})}{(\Delta z_{j-1})^2}, \tag{5.2a}$$

and

$$C_P^{ij} = -[C_R^{ij} + C_T^{ij} - 2K_y^2\sigma_{i,j}] - \frac{2\sigma_{i,j}}{(\Delta x_i)^2}(1 - \alpha\Delta x_i \cos\theta_1) - \frac{2\sigma_{i,j}}{(\Delta z_{j-1})^2}(1 - \alpha\Delta z_{j-1}\cos\theta_2). \tag{5.3a}$$

For the node (N, M) the difference equation is

$$C_L^{ij}\tilde{\phi}_{i-1,j} + C_T^{ij}\tilde{\phi}_{i,j-1} + C_P^{ij}\tilde{\phi}_{i,j} = 2\tilde{Q}\delta(x_s)\,\delta(z_s), \tag{6a}$$

where

$$C_L^{ij} = -\frac{(\sigma_{i-1,j} + \sigma_{i,j})}{(\Delta x_{i-1})^2}, \tag{6.1a}$$

$$C_T^{ij} = -\frac{(\sigma_{i,j-1} + \sigma_{i,j})}{(\Delta z_{j-1})^2}, \tag{6.2a}$$

and

$$C_P^{ij} = -[C_L^{ij} + C_T^{ij} - 2K_y^2\sigma_{i,j}] - \frac{2\sigma_{i,j}}{(\Delta x_{i-1})^2}(1 - \alpha\Delta x_{i-1}\cos\theta_1) - \frac{2\sigma_{i,j}}{(\Delta z_{j-1})^2}(1 - \alpha\Delta z_{j-1} - \cos\theta_2). \tag{6.3a}$$

e. *For the nodes on the left edge of the mesh*

The difference equation for the nodes $(1, j)$ for $j = 2, 3, \ldots, M - 1$, has the form given below

$$C_R^{ij}\tilde{\phi}_{i+1,j} + C_T^{ij}\tilde{\phi}_{i,j-1} + C_B^{ij}\tilde{\phi}_{i,j+1} + C_{ij}^P\tilde{\phi}_{i,j} = 2\tilde{Q}\delta(x_s)\,\delta(z_s), \tag{7a}$$

where

$$C_R^{ij} = \frac{-(\sigma_{i+1,j} + \sigma_{i,j})}{(\Delta x_i)^2}, \tag{7.1a}$$

$$C_T^{ij} = \frac{-2(\sigma_{i,j-1} + \sigma_{i,j})}{(\Delta z_j + \Delta z_{j-1})\,.\,\Delta z_{j-1}}, \tag{7.2a}$$

$$C_B^{ij} = \frac{-2(\sigma_{i,j+1} + \sigma_{i,j})}{(\Delta z_j + \Delta z_{j-1})\,.\,\Delta z_j}, \tag{7.3a}$$

and

$$C_P^{ij} = -[C_L^{ij} + C_R^{ij} + C_B^{ij} - 2K_y^2\sigma_{i,j}] - \frac{2\sigma_{i,j}}{(\Delta x_i)^2}(1 - \alpha\Delta_i x\cos\theta). \tag{7.4a}$$

f. *For the nodes on the right edge of the mesh*

The difference equation for the nodes (N, j) for $j = 2, 3, \ldots, M - 1$, that are on the edge corresponding to $x \to +\infty$, is given below

$$C_L^{ij}\tilde{\phi}_{i-1,j} + C_T^{ij}\tilde{\phi}_{i,j-1} + C_B^{ij}\tilde{\phi}_{i,j+1} + C_P^{ij}\tilde{\phi}_{i,j} = 2\tilde{Q}\delta(x_s)\,\delta(z_s), \tag{8a}$$

where

$$C_L^{ij} = \frac{-(\sigma_{i-1,j} + \sigma_{i,j})}{(\Delta x_{i-1})^2}, \tag{8.1a}$$

$$C_T^{ij} = \frac{-2(\sigma_{i,j-1} + \sigma_{i,j})}{(\Delta z_j + \Delta z_{j-1}) \cdot \Delta z_{j-1}}, \tag{8.2a}$$

$$C_B^{ij} = \frac{-2(\sigma_{i,j+1} + \sigma_{i,j})}{(\Delta z_j + \Delta z_{j-1}) \cdot \Delta z_j}, \tag{8.3a}$$

and

$$C_P^{ij} = -[C_L^{ij} + C_T^{ij} + C_B^{ij} - 2K_y^2\sigma_{i,j}] - \frac{2\sigma_{i,j}}{(\Delta x_{i-1})^2}(1 - \alpha\Delta x_{i-1}\cos\theta). \tag{8.4a}$$

APPENDIX B

Difference Equations for the Boundary Nodes Using Area Discretization Scheme

a. *For nodes located on the ground surface* $(z \to 0)$

The mesh region $\Delta A_{i,j}$ is enclosed by the coutour $L_{i,j}$ defined by the subsections *iii, iv, v, vi, a, b* as shown in figure 2. For all nodes $(i, 1)$, $i = 2, 3, \ldots, N - 1$. The finite difference equation is given by

$$C_L^{ij}\tilde{\phi}_{i-1,j} + C_R^{ij}\tilde{\phi}_{i+1,j} + C_B^{ij}\tilde{\phi}_{i,j+1} + C_P^{ij}\tilde{\phi}_{i,j} = \frac{I}{2}\delta(x_s)\,\delta(z_s), \tag{1b}$$

where

$$C_L^{ij} = \frac{-\Delta z_j \cdot \sigma_{i-1,j}}{2\Delta x_{i-1}}, \tag{1.1b}$$

$$C_R^{ij} = \frac{-\Delta z_j \cdot \sigma_{i,j}}{2\Delta x_i}, \tag{1.2b}$$

$$C_B^{ij} = -\left[\frac{\Delta x_{i-1} \cdot \sigma_{i-1,j} + \Delta x_i \cdot \sigma_{i,j}}{2\Delta z_j}\right], \tag{1.3b}$$

$$A(\sigma_{i,j}, A_{i,j}) = K_y^2\left[\frac{\sigma_{i-1,j} \cdot \Delta x_{i-1} \cdot \Delta z_j}{4} + \frac{\sigma_{i,j} \cdot \Delta x_i \cdot \Delta z_j}{4}\right], \tag{1.4b}$$

and

$$C_P^{ij} = -[C_L^{ij} + C_R^{ij} + C_B^{ij} - A(\sigma_{i,j}, A_{i,j})]. \tag{1.5b}$$

b. *For the top left and right corner nodes on line* $z = 0$

For the nodes (1, 1) and $(N, 1)$, the mesh region $\Delta A_{i,j}$ is bounded by the contour $L_{i,j}$ with the subsections (*iii*, *iv*, *c*, *b*) and (*v*, *vi*, *a*, *c*), respectively. The component of **J** in the z-direction satisfies the Neumann condition $\sigma \cdot \partial\phi/\partial z = 0$, and the component of **J** in the x-direction satisfies the mixed boundary condition

$$\frac{\partial \tilde{\phi}}{\partial x} + \alpha \tilde{\phi} \cos\theta = 0,$$

where

$$\alpha = \frac{K_y K_1(K_y r)}{K_0(K_y r)}$$

and θ is the angle between the radial distance r from the source to the node (i, j) and the outward normal in the x-direction. The finite difference equation for the top left corner node then becomes

$$C_B^{ij} \tilde{\phi}_{i,j+1} + C_R^{ij} \tilde{\phi}_{i+1,j} + C_P^{ij} \tilde{\phi}_{i,j} = \frac{I}{2} \delta(x_s)\, \delta(z_s), \tag{2b}$$

where

$$C_B^{ij} = \frac{-\Delta x_i \sigma_{i,j}}{2\Delta z_j}, \tag{2.1b}$$

$$C_R^{ij} = \frac{-\Delta z_j \sigma_{i,j}}{2\Delta x_i}, \tag{2.2b}$$

$$A(\sigma_{i,j}, A_{i,j}) = K_y^2 \left(\frac{\sigma_{i,j} \cdot \Delta x_i \cdot \Delta z_j}{4}\right), \tag{2.3b}$$

and

$$C_P^{ij} = -[C_B^{ij} + C_R^{ij} - A(\sigma_{i,j}, A_{i,j})] + \frac{\Delta z_j \cdot \sigma_{i,j} \cdot \alpha \cos\theta}{2}. \tag{2.4b}$$

For the top right corner node, we get

$$C_L^{ij} \tilde{\phi}_{i-1,j} + C_B^{ij} \tilde{\phi}_{i,j+1} + C_P^{ij} \tilde{\phi}_{i,j} = \frac{I}{2} \delta(x_s)\, \delta(z_s), \tag{3b}$$

where

$$C_L^{ij} = \frac{-\Delta z_j \cdot \sigma_{i-1,j}}{2\Delta x_{i-1}}, \tag{3.1b}$$

$$C_B^{ij} = \frac{-\Delta x_{i-1} \cdot \sigma_{i-1,j}}{2\Delta z_j}, \tag{3.2b}$$

$$A(\sigma_{i,j}, A_{i,j}) = K_y^2 \left(\frac{(\sigma_{i-1,j} \cdot \Delta x_{i-1} \cdot \Delta z_j}{4} \right), \tag{3.3b}$$

and

$$C_P^{ij} = -[C_L^{ij} + C_B^{ij} - A(\sigma_{i,j}, A_{i,j})] + \frac{\Delta z_j \cdot \sigma_{i-1,j} \cdot \alpha \cos\theta}{2}. \tag{3.4b}$$

c. *For the nodes located on the bottom edge of the mesh* ($z \to \infty$)

The nodes (i, M), $i = 2, 3, \ldots, N-1$, the mesh region $\Delta A_{i,j}$ is bounded by the contour $L_{i,j}$ defined by the subsections *i*, *ii*, *b*, *a*, *vii* and *viii*. The finite difference equation for any of these nodes is

$$C_L^{ij} \tilde{\phi}_{i-1,j} + C_R^{ij} \tilde{\phi}_{i+1,j} + C_T^{ij} \tilde{\phi}_{i,j-1} + C_P^{ij} \tilde{\phi}_{i,j} = \frac{I}{2} \delta(x_s)\, \delta(z_s), \tag{4b}$$

where

$$C_L^{ij} = \frac{-\Delta z_{j-1} \cdot \sigma_{i-1,j-1}}{2\Delta x_{i-1}}, \tag{4.1b}$$

$$C_R^{ij} = \frac{-\Delta z_{j-1} \cdot \sigma_{i,j-1}}{2\Delta x_i}, \tag{4.2b}$$

$$C_T^{ij} = -\left[\frac{\Delta x_{i-1} \cdot \sigma_{i-1,j-1} + \Delta x_i \cdot \sigma_{i,j-1}}{2\Delta z_{j-1}} \right], \tag{4.3b}$$

$$A(\sigma_{i,j}, A_{i,j}) = K_y^2 \left[\frac{\sigma_{i-1,j-1} \cdot \Delta x_{i-1} \cdot \Delta z_{j-1}}{4} + \frac{\sigma_{i,j-1} \cdot \Delta x_i \cdot \Delta z_{j-1}}{4} \right] \tag{4.4b}$$

and

$$C_P^{ij} = -[C_L^{ij} + C_R^{ij} + C_T^{ij} - A(\sigma_{i,j}, A_{i,j})] + \left(\frac{\Delta x_{i-1} \cdot \sigma_{i-1,j-1} + \Delta x_i \cdot \sigma_{i,j-1}}{2} \right) \alpha \cos\theta. \tag{4.5b}$$

d. *For the bottom left and right corner nodes*

For each of the nodes $(1, M)$ and (N, M) the representative mesh region ΔA_{ij} is bounded by the contour line L_{ij} described by the subsections (*i*, *ii*, *b*, *d*) and (*d*, *a*, *vii*, *viii*), respectively. Applying the boundary conditions, the difference equation for the node $(1, M)$ is

$$C_R^{ij} \tilde{\phi}_{i+1,j} + C_T^{ij} \tilde{\phi}_{i,j-1} + C_P^{ij} \tilde{\phi}_{i,j} = \frac{I}{2} \delta(x_s)\, \delta(z_s), \tag{5b}$$

where

$$C_R^{ij} = \frac{-\Delta z_{j-1} \cdot \sigma_{i,j-1}}{2\Delta x_i}, \tag{5.1b}$$

$$C_T^{ij} = \frac{-\Delta x_i \cdot \sigma_{i,j-1}}{2\Delta z_{j-1}}, \tag{5.2b}$$

$$A(\sigma_{i,j}, A_{i,j}) = K_y^2 \left[\frac{\sigma_{i,j-1} \cdot \Delta x_i \cdot \Delta z_{j-1}}{4}\right], \tag{5.3b}$$

and

$$C_P^{ij} = -[C_R^{ij} + C_T^{ij} - A(\sigma_{i,j}, A_{i,j})] + \left(\frac{\Delta x_i \cdot \sigma_{i,j-1}}{2} \cdot \alpha \cos\theta_1 + \frac{\Delta z_{j-1} \cdot \sigma_{i,j-1}}{2} \cdot \alpha \cos\theta_2\right). \tag{5.4b}$$

The difference equation for the bottom right corner node (N, M) is

$$C_L^{ij}\,\tilde{\phi}_{i-1,j} + C_T^{ij}\,\tilde{\phi}_{i,j-1} + C_P^{ij}\,\tilde{\phi}_{i,j} = \frac{I}{2}\,\delta(x_s)\,\delta(z_s), \tag{6b}$$

where

$$C_L^{ij} = \frac{-\Delta z_{i-1} \cdot \sigma_{i-1,j-1}}{2\Delta x_{i-1}}, \tag{6.1b}$$

$$C_T^{ij} = \frac{-\Delta x_{i-1} \cdot \sigma_{i-1,j-1}}{2\Delta z_{j-1}}, \tag{6.2b}$$

$$A(\sigma_{i,j}, A_{i,j}) = K_y^2 \frac{\sigma_{i-1,j-1} \cdot \Delta x_{i-1} \cdot \Delta z_{j-1}}{4}, \tag{6.3b}$$

and

$$C_P^{ij} = -[C_L^{ij} + C_T^{ij} - A(\sigma_{i,j}, A_{i,j})] + \left(\frac{\Delta x_{i-1} \cdot \sigma_{i-1,j-1}}{2} \cdot \alpha \cos\theta_1 + \frac{\Delta z_{j-1} \cdot \sigma_{i-1,j-1}}{2} \cdot \alpha \cos\theta_2\right). \tag{6.4b}$$

θ_2 and θ_1 are the angles between the radial distance r from the source and the x- and z-directions, respectively.

e. *For the nodes on the left edge of the mesh*

For each of the nodes $(1, j)$, $j = 2, 3, \ldots, M-1$, the mesh region ΔA_{ij} is bounded by the contour L_{ij} defined by the subsections *i*, *ii*, *iii*, *iv*, *c*, and *d*. Applying the boundary conditions, we get the difference equation

$$C_R^{ij}\,\tilde{\phi}_{i+1,j} + C_T^{ij}\,\tilde{\phi}_{i,j-1} + C_B^{ij}\,\tilde{\phi}_{i,j+1} + C_P^{ij}\,\tilde{\phi}_{i,j} = \frac{I}{2}\,\delta(x_s)\,\delta(z_s), \tag{7b}$$

where

$$C_R^{ij} = -\left[\frac{\Delta z_j \cdot \sigma_{i,j} + \Delta z_{j-1} \cdot \sigma_{i,j-1}}{2\Delta x_i}\right], \tag{7.1b}$$

$$C_T^{ij} = -\frac{\Delta x_i \cdot \sigma_{i,j-1}}{2\Delta z_{j-1}}, \tag{7.2b}$$

$$C_B^{ij} = -\frac{\Delta x_i \cdot \sigma_{i,j}}{2\Delta z_j}, \tag{7.3b}$$

$$A(\sigma_{i,j}, A_{i,j}) = K_y^2 \left[\frac{\sigma_{i,j-1} \cdot \Delta x_i \cdot \Delta z_{j-1}}{4} + \frac{\sigma_{i,j} \cdot \Delta x_i \cdot \Delta z_j}{4}\right], \tag{7.4b}$$

and

$$C_P^{ij} = -[C_R^{ij} + C_T^{ij} + C_B^{ij} - A(\sigma_{i,j}, A_{i,j})] + \frac{\Delta z_j \cdot \sigma_{i,j} + \Delta z_{j-1} \cdot \sigma_{i,j-1}}{2} \cdot \alpha \cos\theta. \tag{7.5b}$$

f. *For the nodes on the right edge of the mesh*

For each of the nodes (N, j), $j = 2, 3, \ldots, M-1$, the mesh region $\Delta A_{i,j}$ is bounded by the contour $L_{i,j}$ described by the subsections *d*, *c*, *v*, *vi*, *viii*, and *viii*. The difference equation for any of these nodes is

$$C_L^{ij}\,\tilde{\phi}_{i-1,j} + C_T^{ij}\,\tilde{\phi}_{i,j-1} + C_B^{ij}\,\tilde{\phi}_{i,j+1} + C_P^{ij}\,\tilde{\phi}_{i,j} = \frac{I}{2}\,\delta(x_s)\,\delta(z_s), \tag{8b}$$

where

$$C_L^{ij} = -\left[\frac{\Delta z_j \cdot \sigma_{i-1,j} + \Delta z_{j-1} \cdot \sigma_{i-1,j-1}}{2\Delta x_{i-1}}\right], \tag{8.1b}$$

$$C_T^{ij} = -\frac{\Delta x_{i-1} \cdot \sigma_{i-1,j-1}}{2\Delta z_{j-1}}, \tag{8.2b}$$

$$C_B^{ij} = -\frac{\Delta x_{i-1} \cdot \sigma_{i-1,j}}{2\Delta z_j}, \tag{8.3b}$$

$$A(\sigma_{i,j}, A_{i,j}) = K_y^2 \left[\frac{\sigma_{i-1,j-1} \cdot \Delta x_{i-1} \cdot \Delta z_{j-1}}{4} + \frac{\sigma_{i-1,j} \cdot \Delta x_{i-1} \cdot \Delta z_j}{4}\right], \tag{8.4b}$$

and

$$C_P^{ij} = -[C_L^{ij} + C_T^{ij} + C_B^{ij} - A(\sigma_{i,j}, A_{i,j})] + \left(\frac{\Delta z_j \cdot \sigma_{i-1,j} + \Delta z_{j-1} \cdot \sigma_{i-1,j-1}}{2}\right) \cdot \alpha \cos\theta. \tag{8.5b}$$

References

AIKEN, C. L., HASTINGS, D. A., and STURGUL, J. R., 1973, Physical and computer modeling of induced polarization, Geophysical Prospecting 21, 763.

APPARAO, A., ROY, A., and MALLICK, K., 1969, Resistivity model experiments, Geoexploration 7, 45.

COGGON, J. H., 1971, Electromagnetic and electrical modeling by the finite element method, Geophysics 36, 132.

CONCUS, P., and COLUB, G. H., 1973, Use of fast direct methods for the efficient numerical solution of non-separable eliptic equations, SIAM J. Numer. Anal. 10, 1103.

DEY, A., 1967, Model studies on electrical profiling over thick conducting veins, M.Sc. Thesis, Indian Institute of Technology, Kharagpur.

DOUGLAS, J., JR., and RACHFORD, H. H., JR., 1956, On the numerical solution of heat conduction problems in two or three space variables, Trans. Amer. Math. Soc. 82, 421.

FORSYTHE, G. E., and WASOW, W. R., 1960, Finite difference methods for partial differential equations, John Wiley and Sons, Inc., New York.

GUNN, J. E., 1964, The numerical solution of $\nabla \cdot a\nabla u = f$ by a semi-explicit alternating direction iterative method, Numer. Math. 6, 181.

JEPSEN, A. F., 1969, Numerical modeling in resistivity prospecting, Ph.D. Thesis, University of California, Berkeley.

McPhar Geophysics, 1967, Catalogue of resistivity and IP model data, McPhar Geophysics Ltd., Ontario, Canada.

MADDEN, T. R., 1967, Calculations of induced polarization anomalies for arbitrary two-dimensional resistivity structure, paper presented at Symposium on IP, University of California, Berkeley.

MADDEN, T. R., 1971, The resolving power of geoelectric measurements for delineating resistive zones within the crust, Geophys. Monogr. 14, AGU, p. 95.

MARTIN, R. S., and WILKINSON, J. H., 1965, Symmetric decomposition of positive definite band matrices, Numer. Math. 7, 355.

MITCHELL, A. R., 1969, Computational methods in partial differential equations, John Wiley and Sons, Inc., New York.

PEACEMANN, D. W., and RACHFORD, H. H., JR., 1955, The numerical solution of parabolic and elliptic differential equations, Jour. of Soc. Indus. Appl. Math. 3, 28.

SOUTHWELL, R. V., 1946, Relaxation methods in theoretical physics, vol. 1, Clarendon Press, Oxford.

VAN NOSTRAND, R. G., and COOK, K. L., 1966, Interpretation of resistivity data, U.S.G.S. Prof. paper 499.

VARGA, R. S., 1962, Matrix iterative analysis, Prentice-Hall, Englewood Cliffs, New Jersey.

YOUNG, D., 1954, Iterative methods for solving partial difference equations of elliptic type, Trans. Amer. Math. Soc. 76, 92.